

Observing collisions beyond the secular approximation limit

J. Ma^{1,2}, H. Zhang¹, B. Lavorel¹, F. Billard¹, E. Hertz¹, J. Wu², C. Boulet³, J.-M. Hartmann^{4*} and O. Faucher^{1*}

¹Laboratoire Interdisciplinaire CARNOT de Bourgogne,

UMR 6303 CNRS-Université de Bourgogne Franche-Comté, BP 47870, 21078 Dijon, France.

²State Key Laboratory of Precision Spectroscopy, East China Normal University, Shanghai 200062, China.

³Institut des Sciences Moléculaires d'Orsay, CNRS, Université Paris-Sud, Université Paris-Saclay, Orsay F-91405, France.

⁴Laboratoire de Météorologie Dynamique/IPSL, CNRS, Ecole polytechnique, Sorbonne Université, Ecole Normale Supérieure, PSL Research University, F-91120 Palaiseau, France.

*e-mails: olivier.faucher@u-bourgogne.fr, jmhartmann@lmd.polytechnique.fr, jwu@phy.ecnu.edu.cn

Abstract: Energy transfer through quantum coherences plays an essential role in diverse natural phenomena and technological applications, such as human vision¹, light-harvesting complexes², quantum heat engines³, and quantum information and computing⁴. The understanding of the long-lived coherence involved in these phenomena requires a detailed modeling of the system-bath interactions beyond the so-called secular and/or Markovian approximations^{5,6}. Despite continuous theoretical progress on understanding nonsecular dynamics in the last decades, convincing experimental observations are still lacking. By using the laser-kicked molecular rotor as a model system, we here experimentally unveil the nonsecular dynamics in the rotational relaxation of molecules due to thermal collisions. Specifically, the rotational coherence in gas-phase molecules is systematically probed and characterized by the recently discovered rotational alignment echoes^{7,8} featuring a decoherence and dissipation process which can only be explained by the nonsecular quantum master equations for modeling molecular collisions.

Understanding how collisions between molecules change their translational and rotational motions is a fundamental problem of physics that has numerous practical implications. Indeed, most real gas media being at non-negligible pressure, intermolecular interactions affect many observable quantities. At thermodynamic equilibrium, they play a key role in the shape of light absorption and scattering spectra⁹ and in the transports of mass and energy^{10,11}, for instance. When the system has been brought out of equilibrium by some external action (e.g. one or several resonant or nonresonant electromagnetic excitations or a plasma discharge), collisional processes are often the main channel inducing the decoherence bringing it back to equilibrium^{10,12}. Collisional effects have been extensively studied in the spectral domain by looking at the shape of various absorption features⁹. In the time domain, it has been recently shown that the decay of alignment echoes induced by two laser kicks⁷ permits time-resolved measurements of collision-induced rotational changes at short time scales^{8,13}. So far, all quantum models used for the calculation of the effects of decoherence processes due to intermolecular forces are based upon the Markovian and secular approximations^{10,14-16}. These allow to obtain the density matrix $\rho(t)$ describing the evolution of the system when coherences (i.e. non-diagonal elements of ρ) have been created (e.g. by laser pulse(s) as in the present work). Recall that the Markov approximation assumes^{14,15} that all collisions are complete and un-correlated (no memory effects in the system-bath “history”) while the secular approximation assumes¹⁶ that the delay Δt at which the system is observed after the creation of the coherences is much greater than the periods of oscillation of the coherences.

This work provides the first experimental and theoretical evidence that alignment echoes enable to probe an open molecular system at the early stage of its collisional relaxation where the secular approximation breaks down. These echoes⁷ occur after molecules have been suddenly aligned by two successive nonresonant laser excitations. A first short pulse, P_1 , impulsively aligns some of the

molecules along its polarization direction thanks to the anisotropy of the molecular polarizability¹⁷. This results in a peak in the alignment factor $\langle \cos^2(\theta) \rangle(t)$ (θ is the angle between the molecule axis and the laser polarization direction and $\langle \rangle$ denotes the quantum expectation value) that quickly vanishes due to rotational dephasing. After a delay τ_{12} , a second pulse, P_2 , is applied that induces a rephasing process leading to the creation of an echo in the alignment factor at time $\Delta t = 2\tau_{12}$ after P_1 .

The experiment is implemented with the setup depicted in Fig. 1 and further described in the Methods section. After the molecules have been aligned by two laser kicks, the anisotropy of the medium resulting from the reorientation of the molecules is interrogated by a probe pulse. A heterodyne detection is performed so that the measured signal is directly proportional to the convolution of $(\langle \cos^2(\theta) \rangle(t) - 1/3)$ with the temporal envelope of the probe, where $1/3$ is the alignment factor obtained when molecules are randomly oriented. Figure 2a exemplifies the echo features observed in the alignment signal of linear molecules at low pressure. Like any other echo phenomenon, the dominant echo response appears at the symmetric position of P_1 with respect to P_2 along the time axis. It is followed by higher-order and imaginary echoes^{18,19} and revivals. All these structures exhibit an asymmetric temporal shape consisting of a peak resulting from the alignment of the molecules along the polarization of the pump field, and a dip associated with a delocalization of the molecular axes within a plane perpendicular to the field vector. It is only very recently that the collisional dissipation of echoes has been studied^{8,13}, by analyzing the evolution of their amplitudes for various delays at fixed gas density. The interest of this approach to probe the dissipation of the alignment under high pressure conditions where standard alignment revivals cannot be used was demonstrated in Ref. 8. Indeed, revivals restrict the probing of the system to specific times that are tied to the moment of inertia of the molecule. On the contrary, the rotational echo provides much more flexibility, since its time of appearance can be tuned at will by adjusting the delay between P_1 and P_2 . The echo is therefore particularly well suited for interrogating the dynamics of the system at early times, much before the first revival appears. As shown in Fig. 2b, we here look at the echoes from a different point of view, and study the reduction of their amplitudes “ S ” with increasing pressure for fixed values of τ_{12} . Note that all results presented from now on have been recorded in high-pressure mixtures of N_2O gas diluted in 96% of helium. The high concentration of helium, which has been chosen for its weak nonlinear optical properties, allows to overcome the nonlinear propagation effects that would take place in high density pure molecular gases of the same nature. A first indication of the enriched information brought by the echo with respect to the revivals is revealed by Fig. 2c, which shows measured amplitudes of five echoes and two revivals as a function of the density d multiplied by the time of appearance of the considered alignment structure (i.e. the echo or the n^{th} revival). Obviously, the efficiency with which collisions reduce the alignment amplitude is the same for the half and full revival (at 20.2 and 40.4 ps), while it varies significantly for the echoes observed between $\tau_{12} = 1.61$ and 8.58 ps. By repeating the measurements of Fig. 2c for several delays and gas densities, we have been able to extract (see the Methods section) density-normalized characteristic time constants of the echo amplitude decay from exponential fits (see Fig. 2c). The values reported in Fig. 3 show that the echo decay is slow at short times and becomes faster as the delay increases, before a plateau is reached around $2\tau_{12} = 10$ ps. In the plateau region, the echo and the revival share about the same density-normalized characteristic decay time.

In order to explain the difference between the short- and long-time dynamics, we performed numerical simulations of the alignment signal in the presence of collisional dissipation. Starting from equilibrium before the pulses, where the density operator $\rho(t < 0)$ is diagonal with respect to the rotational quantum numbers J (principal) and M (magnetic) and Boltzmannian, the evolution for $t \geq 0$ is obtained from the Liouville-von Neumann equation^{10,14-16}

$$\frac{d\rho}{dt}(t) = -\frac{i}{\hbar}[\mathbf{H}_0 + \mathbf{H}_L(t), \rho(t)] + \left(\frac{d\rho(t)}{dt} \right)_{\text{Coll}}, \quad (1)$$

where \hbar is the Planck constant divided by 2π , \mathbf{H}_0 is the free rotational Hamiltonian and

$$\mathbf{H}_L(t) = -\frac{1}{2}\Delta\alpha E^2(t)(\cos^2\theta - 1/3) \quad (2)$$

describes the non-resonant interaction of the molecule with the linearly polarized field, with $\Delta\alpha$ the anisotropic polarizability and $E(t)$ the temporal envelop of the laser pulse. Assuming a Markovian model of collisions (valid here because N_2O and He interact very shortly and in a very limited range of intermolecular distance²⁰), and neglecting all radiative decays since they occur on a much longer time scale, the matrix elements of the dissipation term read

$$\left(\frac{d\rho_{ij}(t)}{dt}\right)_{\text{Coll}} = -d \sum_{i',j'} \Lambda_{ij,i'j'} \rho_{i'j'}(t), \quad (3)$$

where i and j denote the rotational states $|J,M\rangle$ of the system and $\Lambda_{ij,i'j'}$ are the density-normalized relaxation matrix elements.

In a first step, we use the so-called Bloch model in which dissipative effects are treated within the secular and Markovian approximations. This corresponds to neglecting all elements of the relaxation matrix responsible for transfers among coherences (nondiagonal terms of ρ) and between populations (diagonal elements of ρ) and coherences. Only the $\Lambda_{ij,ij}$ and $\Lambda_{ii,i'i'}$ terms are then kept which are directly related to the rates of population transfer from $|J,M\rangle$ to $|J',M'\rangle$ including inelastic (J -changing) and elastic reorienting (J -conserving, M -changing) processes, as well as the pure dephasing of the coherence which describes the effect of elastic collisions that interrupt the phase of the molecule without quenching it. As shown by the simulations represented by the black line in Fig. 3, the secular theory well reproduces the observed decays of the echoes in the plateau region beyond 10 ps, but does not capture the weaker efficiency of collisions and the variation of the echo decay at short times. This observation seriously questions the validity of the secular approximation during the early dynamics of the system.

For a simple (but realistic) picture of the limits of the secular approximation, let us assume that coherences have been instantaneously generated by a laser pulse at $t=0$. This creates nonzero off-diagonal elements $\rho_{JM,J'M}(t=0^+)$ between states $|J,M\rangle$ and $|J',M'\rangle$, which, in the absence of collisions, then evolve with time according to $\rho_{JM,J'M}(t) = \rho_{JM,J'M}(t=0^+) \exp[-i(E_J - E_{J'})t/\hbar]$, with E_J and $E_{J'}$ the corresponding rotational energies. Let us now assume that collisions induce transfers between coherences and, in particular, from $\rho_{J_1M_1,J'_1M'_1}(t)$ to $\rho_{J_0M_0,J'_0M'_0}(t)$ with a real valued rate constant. Under some approximations, it can be shown that the relative change of $\rho_{J_0M_0,J'_0M'_0}(t)$ due to transfers from $\rho_{J_1M_1,J'_1M'_1}(t)$ at time t after the laser pulse is

$$\text{Re} \left[\frac{\Delta\rho_{J_0M_0,J'_0M'_0}(t)}{\rho_{J_0M_0,J'_0M'_0}(t)} \right] = B \text{sinc} \left[(\omega_{J_1J'_1} - \omega_{J_0J'_0})t \right], \quad (4)$$

where $\text{Re}[\dots]$ denotes the real part, B is a constant, $\text{sinc}[\dots]$ designates a cardinal sine and $\omega_{JJ'} \equiv (E_J - E_{J'})/\hbar$. It is obvious from Equation (4) that, as $|\omega_{J_1J'_1} - \omega_{J_0J'_0}|t$ gets larger than a few times π , the transfers between coherences become negligible when compared to the total loss. In order to be more quantitative, let us consider the case of N_2O . Since only the real part of $\rho_{JM,J'M}(t)$ with $J'=J \pm 2$ contributes to the echo amplitude (see the Methods section), we below focus on such elements and limit ourselves to the most populated state $J_0=15$ at $T=300$ K. The quantity in Equation (4) is plotted in Fig. 4 for $J_0=15$, $J'_0=17$, $J'_1=J_1+2$ and $J_1=17, 19, 21$, and 23 (we keep $|J_0 - J_1|$ even because of the collisional selection rule), where all values have been normalized to unity at $t=0$. As

can be seen, transfers between coherences indeed decrease rapidly. They are significant before about 5 ps and practically negligible above 10 ps, a behavior qualitatively consistent with the difference between the experimental results and the secular predictions in Fig 3.

In order to go further, computations of the echo decays have been carried by solving equations (1)-(3) now keeping all collisional transfers channels and thus accounting for secular and nonsecular terms. The required relaxation matrix elements have been constructed using the Infinite Order Sudden model, where the consistency with the rates used previously within the secular approximation²¹⁻²³ is demonstrated. Unfortunately, due to computer-time and -memory limitations, nonsecular calculations at room temperature, which require to include N₂O J values up to $J_{\text{Max}}=60$, were not tractable (which is not the case when the secular approximation is used). Hence, we carried calculations for $T=100$ K and $J_{\text{Max}}=38$, conditions for which predictions for 6 densities and 21 delays τ_{12} could be completed in a “reasonable” time. The results of this exercise, in which we used rates computed at 295 K but initial populations defined at 100 K, are displayed in Fig. 3. Note that comparing the secular results at 100 K and 300 K shows that limiting computations to $T=100$ K and $J_{\text{Max}}=38$ only slightly affects the prediction (by 10 %). Figure 3 confirms that the nonsecular terms corresponding to the transfers among coherences as well as between populations and coherences globally contribute to reduce the pressure-induced echo decay at short times. As time goes by, the averaging out of these terms (see Fig. 4) results in a decrease of the predicted decay rate toward a plateau, in perfect agreement with the measurements. Note that the convergence of the nonsecular results toward the delay-independent secular ones (Fig. 3) explains the close similarity of the decays of the revivals and of the echo for large delays experimentally observed (Fig. 2c).

Collisional dynamics of rotationally excited N₂O molecules diluted in helium gas has been investigated using alignment echoes. The latter enable to probe the system very soon after its stimulation by two laser kicks, on a time scale that is comparable to the time interval between successive collisions at the high densities used in the measurements. This unprecedented scrutiny enables to our knowledge the first observation of collisional transfers occurring in the nonsecular regime and leading to a slowing-down of the decoherence of the system lasting for a few picoseconds. This observed longevity of coherences challenges the traditional wisdom that interactions with the environment universally lead to decoherence only, and boosts the theoretical revisiting of the quantum master equations normally used to describe the system-bath interactions. It also opens renewed perspectives, through pure time-domain experiments, for our understanding of collisional processes and tests of rotational relaxation models.

Methods

Experimental set-up. The experiment is based on a chirped femtosecond Ti:Sapphire amplifier delivering 800 nm light pulses with a repetition rate of 1 kHz and a duration of 100 fs. The output of this laser is first separated into a pump and a probe beam. The pump beam, used for impulsive alignment, is directed through a Mach-Zehnder interferometer producing two linearly-polarized collinearly-propagating pulses P_1 and P_2 with a time delay controlled by a motorized stage. In order to reduce the perturbation of the detection by the light of the pump pulses scattered by the molecules and the cell windows, the probe beam is frequency doubled with a type I BBO crystal before being sent through a second motorized delay line. For the purpose of the birefringence detection, its polarization is rotated by 45° with respect to the pump pulses. The pump and probe beams are both focused in a high-pressure static cell by the same lens ($f=100$ mm) in a noncolinear geometry leading to a crossing angle of 4° at focus. The intensities of P_1 and P_2 are estimated around 20 and 13 TW/cm², respectively. After filtering out the 800 nm photons and collecting the 400 nm light with a second lens, the transmitted probe light is analyzed by a low noise balanced detection ensuring a heterodyne detection. The latter is achieved by combining a quarter-wave plate and a Wollaston prism separating the vertical and horizontal polarization components that are then independently measured by two

connected head-to-tail photodiodes. All measurements were made at room temperature (295 K) with various total pressures up to 25 bar.

Computations. The density matrix ρ was initialized, before the first laser pulse, to its equilibrium value at 100 K and 295 K (see text). Its evolution with time was then obtained by solving Equations (1) and (2) for a 100 fs Gaussian pulse envelop (FWHM) and the same pulses intensities as in the experiments, using the anisotropic polarizability²⁴ $\Delta\alpha=19.8 \text{ a}_0^3$ and the rotational constant $B = 0.419 \text{ cm}^{-1}$ of N_2O . The collisional term was computed using Equation (3), with rates $\Lambda_{J_1 M_1, J_1' M_1' \rightarrow J_0 M_0, J_0' M_0'}$ constructed using the Infinite Order Sudden Approximation (IOSA). Considering that all operators are diagonal in M , only the $\langle JM | \rho(t) | J' M \rangle$ terms were computed. From knowledge of these density matrix elements, the alignment factor was computed from

$$\langle \cos^2 \theta - 1/3 \rangle = \sum_{J, M} \langle JM | \rho(t) \cos^2 \theta | JM \rangle = \sum_{J, M, J'} \langle JM | \rho(t) | J' M \rangle \langle J' M | \cos^2 \theta | JM \rangle$$

with $\langle J' M | \cos^2 \theta | JM \rangle = \frac{2}{3} \sqrt{(2J+1)(2J'+1)} \begin{pmatrix} J & 2 & J' \\ 0 & 0 & 0 \end{pmatrix} \begin{pmatrix} J & 2 & J' \\ M & 0 & -M \end{pmatrix}$, where $(:::)$ is a 3J symbol. Note that this implies $J'-J=0, \pm 2$.

Data analysis. For each delay τ_{12} between the laser pulses P_1 and P_2 , the measured and computed alignment factors for various gas densities d were analyzed as follows. The variation with d of the peak-to-dip amplitude S of the echo (see Fig. 2b) was (nicely, see Fig. 2c) least-squares fitted by $S(d, \tau_{12}) = A(\tau_{12}) \exp[-d/d_0(\tau_{12})]$ floating $A(\tau_{12})$ and $d_0(\tau_{12})$. A density-normalized decay time constant was then defined as $\tau_E(\tau_{12}) = 2\tau_{12}d_0(\tau_{12})$, considering the fact that the echo appears at $t=2\tau_{12}$ after the time origin defined by P_1 . For the revivals, the same approach was used except that P_2 was turned off, and a density-normalized time constant was determined for each of them from the decay of their amplitude with density using $\tau_R(t_R) = t_R d_0(t_R)$, where t_R is the time delay between the revival and P_1 .

References

1. Schoenlein, R. W., Peteanu, L. A., Mathies, R. A., & Shank, C. V. The First Step in Vision: Femtosecond Isomerization of Rhodopsin. *Science* **254**, 412-415 (1991).
2. Engel, G.S., et al. Evidence for wavelike energy transfer through quantum coherence in photosynthetic systems. *Nature* **446**, 782-786 (2007).
3. Scully, M. O., Chapin, K. R., Dorfman, K. E., Kim, M. B., & Svidzinsky A. Quantum heat engine power can be increased by noise-induced coherence. *Proceedings of the National Academy of Sciences* **108**, 15097-15100 (2011).
4. Monroe, C. Quantum information processing with atoms and photons. *Nature* **416**, 238-246 (2002).
5. Lambert, N., et al. Quantum biology. *Nat. Phys.* **9**, 10-18 (2013).
6. Breuer, H.-P., Laine, E.-M., Piilo, J., & Vacchini, B. Colloquium: Non-Markovian dynamics in open quantum systems. *Rev. Mod. Phys.* **88**, 021002 (2016).
7. Karras, G., et al. Orientation and Alignment Echoes. *Phys. Rev. Lett.* **114**, 153601 (2015).
8. Zhang, H., et al. Rotational Echoes as a Tool for Investigating Ultrafast Collisional Dynamics of Molecules. *Phys. Rev. Lett.* **122**, 193401 (2019).
9. Hartmann, J.-M., Boulet, C., & Robert, D. *Collisional Effects On Molecular Spectra. Laboratory Experiments And Models, Consequences For Applications* (Elsevier, Amsterdam, 2008).
10. May, V., & Kuhn, O. *Charge and Energy Transfer Dynamics in Molecular Systems* (Wiley-VCH, Weinheim, 2011).
11. Hirschfelder, J. O., Curtiss, C. F., & Bird, R. B.. *Molecular Theory of Gases and Liquids*, second edition (Wiley, New-York, 1964).

12. Boyd, I. D., & Schwartzentruber, T. E. *Nonequilibrium Gas Dynamics and Molecular Simulation* (Cambridge University Press, Cambridge, 2017).
13. Rosenberg, D., Damari, R., & Fleischer S. Echo Spectroscopy in Multilevel Quantum-Mechanical Rotors. *Phys. Rev. Lett.* **121**, 234101 (2018).
14. Breton, J., Hardisson, A., Mauricio, F., & Velasco, S. Relaxation of quantum systems weakly coupled to a bath. I; Total time ordering cumulant and partial time ordering cumulant non-Markovian theories. *Phys. Rev. A* **30**, 542-552 (1984)
15. Kosloff, R. Quantum thermodynamics and open-systems modeling. *J. Chem. Phys.* **150**, 204105 (2019)
16. Cohen-Tannoudji, C., Dupont-Roc, J., & Grynberg, G. *Atom-Photon Interactions. Basic Processes and Applications* (Wiley-VCH, Weinheim, 1998).
17. Stapelfeldt, H and Seideman, T. Colloquium: aligning molecules with strong laser pulses. *Rev. Mod. Phys.* **75**, 543 (2003).
18. Karras, G., et al. Experimental observation of fractional echoes. *Phys. Rev. A* **94**, 033404 (2016).
19. Lin, K., et al. Echoes in space and time. *Phys. Rev. X* **6**, 041056 (2016).
20. Wang, L., Xie, D., & Le Roy, R. J. New four-dimensional ab initio potential energy surface for N₂O–He and vibrational band origin shifts for the N₂O–He_N clusters with N=1–40. *J. Chem. Phys.* **137**, 104311 (2012).
21. Hartmann, J.-M., & Boulet, C. Quantum and classical approaches for rotational relaxation and nonresonant laser alignment of linear molecules: A comparison for CO₂ gas in the nonadiabatic regime. *J. Chem. Phys.* **136**, 184302 (2012).
22. Vieillard, T., et al. Field-free molecular alignment for probing collisional relaxation dynamics. *Phys. Rev. A* **87**, 023409 (2013).
22. Ramakrishna, S., & Seideman, T. Intense Laser Alignment in Dissipative Media as a Route to Solvent Dynamics. *Phys. Rev. Lett.* **95**, 113001 (2005).
24. Hohm, U. Dispersion of polarizability anisotropy of H₂, O₂, N₂O, CO₂, NH₃, C₂H₆, and cyclo-C₃H₆, and evaluation of isotropic and anisotropic dispersion-interaction energy coefficients. *Chem. Phys.* **179**, 533-541 (1994).

Acknowledgments

The work was supported by the ERDF Operational Programme – Burgundy 2014/2020 and the EIPHI Graduate School (contract "ANR-17-EURE-0002"). J. Ma acknowledges the support from the China Scholarship Council (CSC). J.-M. Hartmann benefited, for the computer simulations, from the IPSL mesocenter ESPRI facility which is supported by CNRS, UPMC, Labex L-IPSL, CNES, and Ecole Polytechnique. J.Wu acknowledges the support by the National Key R&D Program (Grant No. 2018YFA0306303) and the NSFC (Grant Nos. 11425416 and 11834004).

Author contributions

O.F. with J.-M.H. planned the project and wrote the manuscript. H.Z. and B.L., with the assistance from J.M. and F.B., designed and installed the experiment. J.M. carried out the measurements. B.L. and J.M. analyzed the data. J.-M.H. and C.B. developed the theory and carried out the simulations. All authors took part in regular discussions and contributed to the final manuscript.

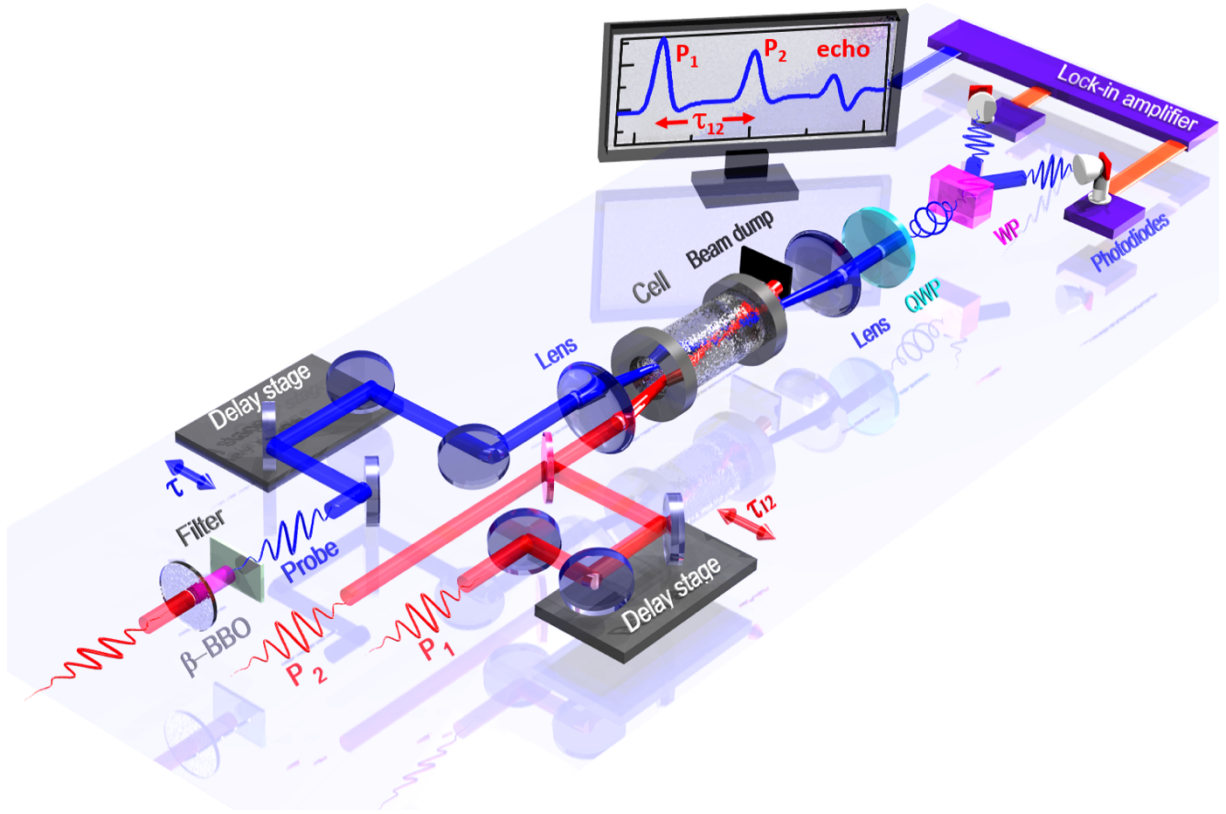


Figure 1: Schematic representation of the experimental set-up. N₂O gas molecules contained in a room-temperature high-pressure gas cell are impulsively aligned by two time-delayed 800 nm pulses P_1 and P_2 . The induced rotational dynamics is measured through the time-dependent birefringence experienced by a 400 nm probe pulse. The detection uses two photodiodes connected head-to-tail to a lock-in amplifier, delivering a signal proportional to the part of the probe field that has been depolarized by the aligned molecules. The image reproduced on the computer screen illustrates the alignment echo signal produced by the two time-delayed strong laser kicks; QWP, quarter-wave plate; WP, Wollaston prism.

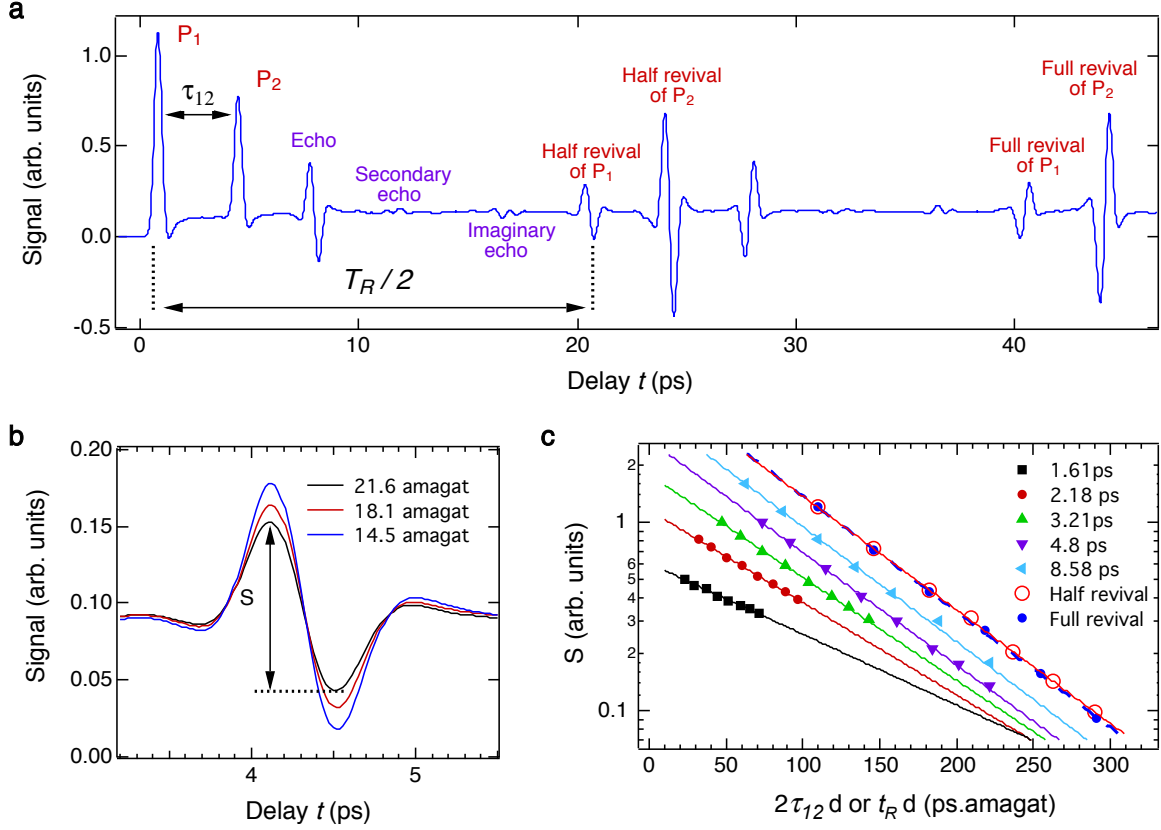


Figure 2: Rotational structures of N_2O aligned by two laser kicks. **a**, Alignment signal recorded in pure N_2O gas at low pressure by scanning the temporal delay between the first aligning pulse P_1 (at $t=0$) and the probe pulse over slightly more than the full rotational period $T_R=40.4$ ps of the molecule. The peaks identified by P_1 and P_2 correspond to the transient alignment signal produced by the two pulses separated by the delay τ_{12} . The main echo is generated at $t=2\tau_{12}$, with the secondary echo observable at $t=3\tau_{12}$, and the imaginary echo produced at $T_R/2 - \tau_{12}$ (equivalent features also appearing at times shifted by $+T_R/2$). In addition to echoes, other transients corresponding to the standard half and full alignment revivals of P_1 (at $T_R/2$ and T_R) and P_2 (at $T_R/2 + \tau_{12}$ and $T_R + \tau_{12}$) are also observed. **b**, Alignment traces of N_2O diluted in He measured at various densities around the main echo at $2\tau_{12}$ for $\tau_{12}=2.18$ ps. The amplitudes S of the alignment structures are measured from peak to dip. **c**, Amplitudes of the half revival (open red circles), full revival (full blue circles), and of the main echo for five different values of the delay τ_{12} versus the gas density d multiplied by the time of observation t_R ($T_R/2$ or T_R) and $2\tau_{12}$ for the revivals and echo, respectively, expressed in picosecond amagat (ps.amagat, with $1 \text{ amagat} = 2.687 \cdot 10^{25} \text{ molec/m}^3$) units. The lines indicate the best exponential fits.

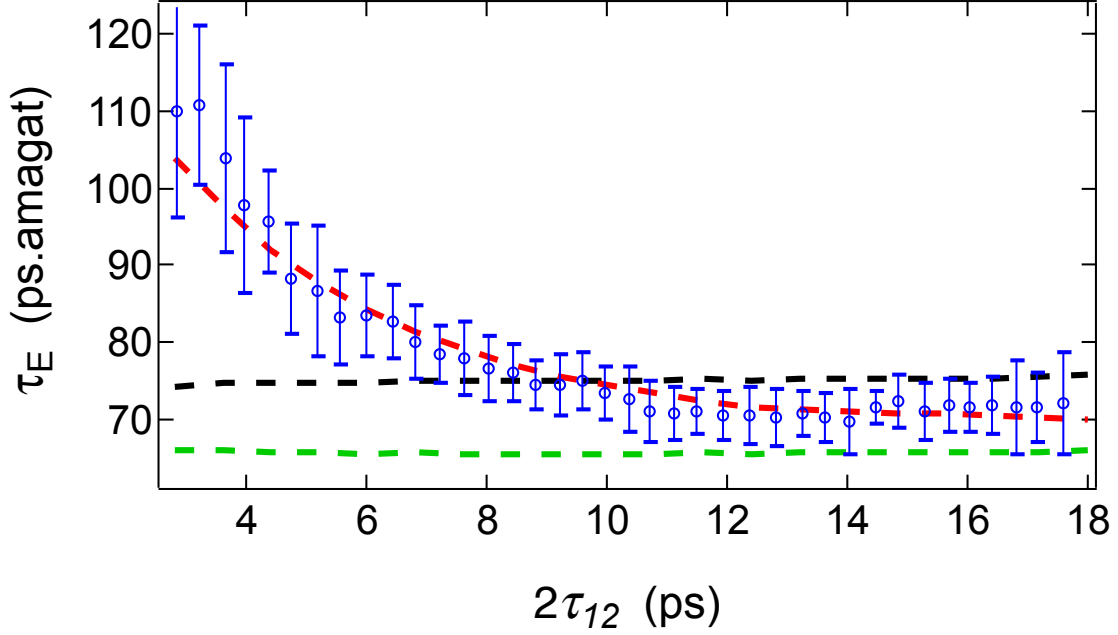


Figure 3: Time constants of collisional dissipation of N_2O . The blue circles with error bars (representing two standard deviations of the mean) are the density-normalized decay time constants τ_E of the echoes deduced from the measurements of the alignment signal recorded at various $\text{N}_2\text{O}(4\%)+\text{He}(96\%)$ gas densities and fixed delays τ_{12} between the two pulses. The dashed lines denote the results of simulations conducted by solving the density matrix equations for molecules impulsively aligned by two short laser pulses and interacting with each other through collisions. The green and black dashed lines have been obtained using the standard Bloch equations (i.e. using the secular approximation) with initial N_2O rotational populations corresponding to temperatures of $T=100$ K and 295 K, respectively. The red dashed line represents the results obtained, for populations associated with $T=100$ K (see text), using the nonsecular Redfield equations, i.e. including all relaxation terms in Equation (3).

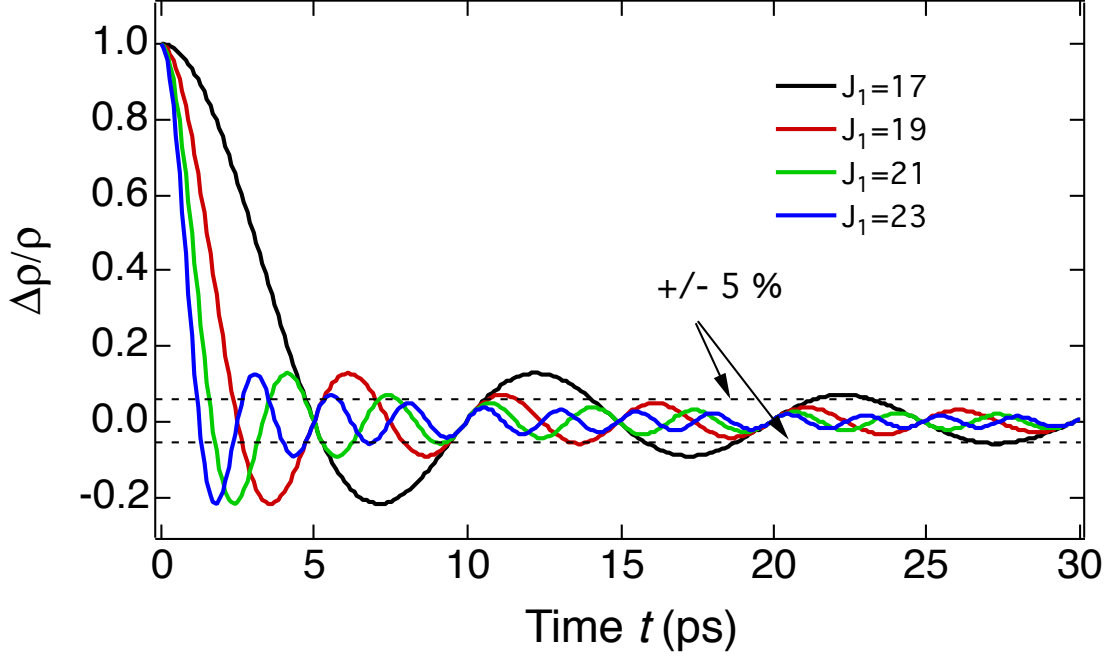


Figure 4: Coherence transfer through collisions. Relative modification of the $\rho_{J_0 M_0, J_0+2M_0}(t)$ coherence for $J_0=15$ induced by collisional transfers from the coherences $\rho_{J_1 M_1, J_1+2M_1}(t)$ with $J_1=17$ (black), $J_1=19$ (red), $J_1=21$ (green), and $J_1=23$ (blue), all normalized to unity at $t=0$. This simple modeling of coherence transfers considering only few rotational states around the most populated state of N_2O at 300 K reveals that during the short time evolution of the system, exchanges between coherences are efficient, which slow down the decay of the alignment factor with respect to what would be obtained using the secular approximation that neglects these collisional transfers and only takes the losses into account.